Available online at www.sciencedirect.com
ScienceDirect
Geochimica et Cosmochimica Acta 71 (2007) 3915–3925
Geochimica et Cosmochimica Acta
www.elsevier.com/locate/gca

Cr diffusion in orthopyroxene: Experimental determination, ^{53}Mn–^{53}Cr thermochronology, and planetary applications

Jibamitra Ganguly [a,*], Motoo Ito [b,1], Xiaoyu Zhang [a]

[a] Department of Geosciences, University of Arizona, Tucson, AZ 85721, USA
[b] Radioisotope Centre, University of Tokyo, 2-11-16 Yayoi, Bunkyo-Ku, Tokyo 113-0032, Japan

Received 2 January 2007; accepted in revised form 29 May 2007; available online 12 June 2007

Abstract

We have determined Cr diffusion coefficients (D) in orthopyroxene parallel to the a-, b-, and c-axial directions as a function temperature at $f(O_2)$ corresponding to those of the wüstite–iron (WI) buffer. Diffusion is found to be significantly anisotropic with $D(//c) > D(//b) > D(//a)$, conforming to an earlier theoretical prediction. Increase of $f(O_2)$ from WI buffer conditions to 4.5 log unit above the buffer at 950 and 1050 °C leads to decrease of D(Cr) by a factor of two to three, possibly suggesting significant contribution from an interstitial diffusion mechanism. We have used the diffusion data to calculate the closure temperatures (T_c) of the Mn–Cr decay system in orthopyroxene as a function of initial temperature (T_0), grain size (a) and cooling rate for spherical and plane sheet geometries. We also present graphical relations that permit retrieval of cooling rates from knowledge of the resetting of Mn–Cr ages in orthopyroxene during cooling, T_0 and a. Application of these relations to the Mn–Cr age data of the cumulate eucrite Serra de Magé yields a T_c of 830–980 °C, and cooling rates of 2–27 °C/Myr at T_c and ~1–13 °C/Myr at 500 °C. It is shown that the cooling of Serra de Magé to the closure temperature of the Mn–Cr system took place at its original site in the parent body, and thus implies a thickness for the eucrite crust in the commonly accepted HED parent body, Vesta, of greater than 30 km. This thickness of the eucrite crust is compatible only with a model of relatively olivine-poor bulk mineralogy in which olivine constitutes 19.7% of the total asteroidal mass.

1. INTRODUCTION

The Mn–Cr decay system, in which the short-lived nuclide ^{53}Mn decays to ^{53}Cr by electron capture, and has a half-life of 3.7 Myr, provides an important tool for dating early solar system objects that show radiogenic ^{53}Cr ($^{53}Cr^*$). Excess ^{53}Cr relative to the terrestrial abundance, which is non-radiogenic, has been detected in the two most abundant meteoritic minerals, olivine and orthopyroxene, and in addition also in spinels and plagioclase from several meteorites (e.g., Hutcheon et al., 1998; Lugmair and Shukolyukov, 1998; Nyquist et al., 2001; Sugiura, 2002). Although ^{53}Mn is a short-lived nuclide, its half-life is relatively long in comparison to those of other short-lived nuclides such as ^{26}Al (0.73 Myr), ^{41}Ca (0.10 Myr), ^{10}Be (1.5 Myr). As discussed by McKeegan and Davis (2004), this relatively long half-life of ^{53}Mn (among the short-lived radionuclides), along with the fact that Mn and Cr are reasonably abundant elements, make the ^{53}Mn–^{53}Cr decay system an important chronological tool to explore the time period from nebular events to accretion and differentiation of early-formed planetesimals.

A mineral age determined by any decay system corresponds to the time period since the closure of the decay products within the mineral grains during cooling. The closure temperature, T_c, of a specific decay system in a mineral depends on a number of factors, namely, diffusion kinetic properties of the system, cooling rate of the host rock, and size and geometry of the mineral grains used for dating

* Corresponding author. Fax: +1 520 621 2672.
E-mail addresses: ganguly@email.arizona.edu (J. Ganguly), motoo.ito-1@nasa.gov (M. Ito).
[1] Present address: NASA, Johnson Space Center ARES, Mail Code KR 2101 NASA Parkway, Houston, TX 77058, USA.

0016-7037/$ - see front matter © 2007 Elsevier Ltd. All rights reserved.
doi:10.1016/j.gca.2007.05.023

(Dodson, 1973). In addition, for slowly diffusing systems T_c also depends on the initial temperature, T_0, at the onset of cooling (Ganguly and Tirone, 1999, 2001). A proper interpretation of mineral age requires an unambiguous characterization of T_c as a function of the above variables. We have thus undertaken a systematic study of Cr diffusion in meteoritic minerals, especially in the two most abundant ones, olivine and orthopyroxene, to properly quantify the mineral closure temperatures. As shown elsewhere (Ganguly and Tirone, 1999, 2001; Ito and Ganguly, 2006), these data also enable us to develop thermochronological formulations that permit retrieval of cooling rates from T_0, grain size, and the extent of resetting of age or age loss between T_0 and T_c.

The Cr diffusion data in olivine and the related closure temperature and thermochronological formulations have been recently presented by Ito and Ganguly (2006). These results are also used to retrieve the cooling rate of the pallasite (stony-iron meteorite) Omolon from the Mn–Cr age of olivine and thereby to constrain its burial depth, which corresponds to the core-mantle boundary, in the parent body. In this work, we present Cr diffusion data in orthopyroxene and the related closure temperature and thermochronological formulations. These results are applied to constrain the cooling rates and burial depths of a cumulate eucrite sample, and thus to provide constraints on the mineralogy and structure of the commonly accepted parent body, asteroid Vesta.

2. EXPERIMENTAL AND ANALYTICAL METHODS

2.1. Starting material and experimental method

The orthopyroxene crystals used in this work are gem quality natural crystals from Sri Lanka with ~96% $MgSiO_3$ (enstatite) content. The composition of a typical crystal, as determined by spot analyses in an electron microprobe, is given in Table 1. Since diffusion in orthopyroxene is expected to be anisotropic (Ganguly and Tazzoli, 1994; Schwandt et al., 1998), with the three principal diffusion axes being parallel to the crystallographic axes, the orthopyroxene crystals were oriented in a single crystal diffractometer and cut normal to the *a*-, *b*-, and *c*-crystallographic directions. The oriented cut faces were then polished stepwise to mirror finish, following the procedure described in Ito and Ganguly (2006).

Table 1
Electron probe data (average of six analyses) of enstatite used in the diffusion study

Oxide	wt% (1σ)		Atom proportion (1σ)
Na_2O	0.0099 (0.0066)	Na	0.0006 (0.0004)
SiO_2	57.4595 (0.1984)	Si	1.9407 (0.0023)
MgO	38.0118 (0.0616)	Mg	1.9139 (0.0037)
Al_2O_3	2.4380 (0.0460)	Al	0.0970 (0.0019)
CaO	0.1509 (1.052)	Ca	0.0055 (0.0002)
MnO	0.0185 (0.0141)	Mn	0.0005 (0.0004)
FeO	1.8049 (0.0567)	Fe	0.0510 (0.0016)
TiO_2	0.0306 (0.0306)	Ti	0.0008 (0.0005)
Cr_2O_3	0.0049 (0.0022)	Cr	0.0001 (0.0001)
Total	99.9289	Cations	4.0102
		Oxygen	6.0000

The experiments were carried out in a vertical gas mixing furnace in which a desired $f(O_2)$ condition was imposed by a computer controlled flowing mixture of CO and CO_2 and cross-checked by a zirconia sensor, as described by Ito and Ganguly (2006). Prior to the tracer diffusion experiments, the polished samples were thermally pre-annealed at T-$f(O_2)$ conditions at or close to those of the diffusion experiments in order to equilibrate the point defect concentrations of the crystals to the experimental condition or nearly so, and also to anneal the effects of strain caused by the polishing process. A thin layer of Cr was deposited on the polished surface of a pre-annealed sample by thermal evaporation under very high vacuum conditions. The sample was then inserted quickly from the top to the hot spot of the furnace that was already set to the desired T-$f(O_2)$ condition of an experiment. The furnace was completely sealed immediately after the insertion of the sample.

A new modification to the furnace involves forced recirculation of the gas mixture into the furnace and periodic venting of gas through a pressure release valve. This procedure greatly reduces the gas consumption and thus makes it possible to carry out diffusion experiments over a long period of time. Furthermore, we are now able to use much greater flow rate of CO_2 compared to what we were able to achieve earlier, and were thus able to study the effect of $f(O_2)$ on the diffusion kinetics over significantly larger range of $f(O_2)$ conditions compared to the earlier study of Ito and Ganguly (2006) on Cr diffusion in olivine.

2.2. Measurement of diffusion profiles

The experimentally induced diffusion profiles were measured by depth-profiling in an ion microprobe in one of two ion probe facilities, the Cameca ims-6f SIMS at the University of Tokyo and the Cameca ims-3f SIMS at the Arizona State University, with most of the measurements being carried out in the former facility. To minimize electrostatic charging of a sample by the primary ion beam irradiation, a thin film (~30 nm) of either Pd (Tokyo laboratory) or Au (ASU laboratory) was deposited on a sample surface. The Cr diffusion profiles were measured as the spatial variation of ^{53}Cr along with, occasionally, that of ^{50}Cr. In addition, spatial variation of the non-diffusing species ^{56}Fe, ^{30}Si, and ^{104}Pd or ^{197}Au were also measured simultaneously during the sputtering process. In several analyses, ^{26}Mg was measured instead of ^{50}Cr. The purpose of measuring the non-diffusing species was to help us locate the thin film and crystal surfaces and monitor the stability of the analyses. A typical set of analytical data is shown in Fig. 1.

Because of the mixing effect during depth profiling, the intensity of the Au or Pd layer gets smeared over certain distance. It is assumed that the surface of Cr thin film, over which the metal thin films were deposited, lies approximately at half-intensity for the counts for ^{104}Pd or ^{197}Au (Fig. 1a). The sample surface is assumed to be located in between this distance and that at which a non-diffusing species achieved plateau intensity. Since all non-diffusing species do

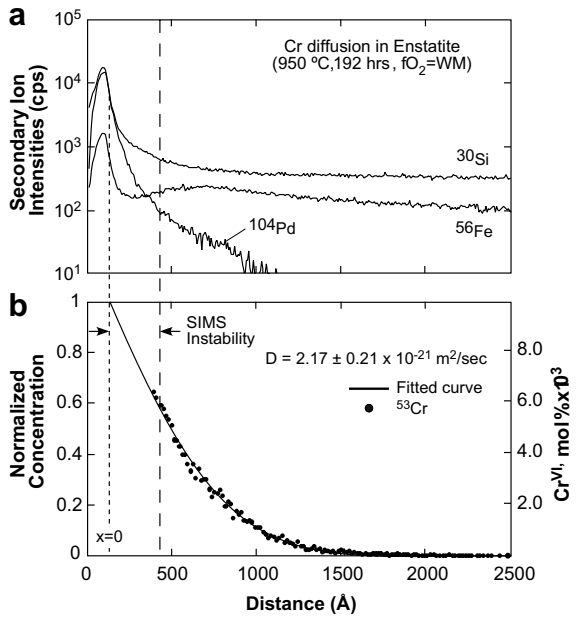

Fig. 1. Typical SIMS depth profile (dots) of ^{53}Cr parallel to the *c*-axis in enstatite that was annealed at 1 bar, 950 °C and $f(O_2)$ of WI buffer, along with those of ^{30}Si, ^{56}Fe, and ^{104}Pd. The thin film surface was located to coincide with depth at which the intensity of the coating material, ^{104}Pd, reduces to half the peak value, whereas the depth of stabilization of the secondary ion counts for non-diffusing species, ^{30}Si and ^{56}Fe, were used to determine the initial analytical cycles of instrumental instability. The crystal surface ($x = 0$) typically coincides or lies very close to the ^{30}Si peak, which for this sample almost coincides with position of half-intensity of ^{104}Pd. The model fit to the ^{53}Cr data, according to the homogeneous infinite source model, is shown by a solid line.

not achieve plateau intensity at the same time, the distance for the first plateau intensity is chosen for this purpose. In an earlier study (Ganguly et al., 1998), in which the diffusing element was deposited on the crystal surface from a dilute HCl solution, we found that the sharp drop of Cl counts to almost to zero coincided with the peak of ^{30}Si that is always present at somewhat shorter distance from the surface than that for its plateau value. We, therefore, fixed the crystal surface to the position of the ^{30}Si peak.

3. RESULTS AND DISCUSSION

3.1. Diffusion coefficients and anisotropy

The solid line fitted to the ^{53}Cr diffusion data in Fig. 1b represents the model fit to the data according to the solution of diffusion equation for a semi-infinite medium and a semi-infinite source. In general, we used both semi-infinite and depleting source solutions (Crank, 1975), interfacing those to an optimization program that yields the best combination of values of the surface concentration, C_S, and diffusion coefficient, D (Tirone et al., 2005). This procedure was dictated by the fact that the surface concentration cannot be determined from the SIMS data since it takes several analytical cycles to achieve instrumental stability. As we have found in other studies of tracer diffusion using similar experimental procedure (Ito and Ganguly, 2004, 2006; Tirone et al., 2005), the solution for semi-infinite source always yielded better fits to the experimental data than those for the depleting source. Thus, the D values retrieved from the former model are taken to be the appropriate values for Cr diffusion in orthopyroxene. We estimated the mol % of Cr in the octahedral site of orthopyroxene as a function of distance within the diffusion zone. These results, which are illustrated on the right hand vertical axis of Fig. 1b, were obtained from the ratio of secondary ion intensities of Cr and Si according to the method of Ito and Ganguly (2006). The diffusion data along with the experimental conditions are summarized in Table 2.

The statistical errors in the retrieved D values were determined by considering (a) the scatter of the normalized concentration data around the model fits (Fig. 1b) and (b) the effects of errors in the measurement of crater depths. The variance of D, σ_D^2, was calculated approximately as $(\sigma_{D(a)})^2 + (\sigma_{D(b)})^2$. The standard error of D due to the scatter of data, i.e. $\sigma_{D(a)}$, was calculated according to the numerical method of Tirone et al. (2005), whereas that resulting from the error in crater depth measurement was approximately calculated from the relation that for a fixed time, $D \propto X^2$, where X is the length of the diffusion profile. Typically, the contribution of $\sigma_{D(b)}$ to the overall σ_D turned out to be negligible.

Time series experiments were conducted at 1100 and 950 °C at constant $f(O_2)$ condition to check if there is any contribution from non-diffusive transport process that could result in a variation of the retrieved D values with time. The results of these experiments are illustrated in Fig. 2. Within errors of the retrieved values, D(Cr) at 1100 °C is found to be independent of time. On the other hand, in the 950 °C time series, there is a change of $\log D$ by ~0.4 between 46 and 97 h, but there is essentially no change of D between 97 and 192 h experiments. We, thus, suggest that the initial variation of the D value is due to error of 46 h. experiment, perhaps a slightly higher sample temperature than recorded by the thermocouple, rather than a result of interference from chemical reaction.

Fig. 3 shows the diffusion data parallel to *a*-, *b*-, and *c*-axial directions of orthopyroxene. All three samples were annealed simultaneously at 1000 °C for 48 h at $f(O_2)$ condition corresponding to that of the WI buffer by a flowing mixture of CO and CO_2. In addition, Cr thin films were also deposited simultaneously by thermal evaporation on all three samples, and these were again pre-annealed simultaneously at 1000 °C for 48 h. The ion probe measurements were carried out under identical conditions in the same session. The results show clear diffusion anisotropy with $D(//c) > D(//b) > D(//a)$. The observed anisotropy is in qualitative agreement with the prediction of Ganguly and Tazzoli (1994) for diffusion of octahedral cations in orthopyroxene.

3.2. Arrhenian relations and comparison with olivine

Fig. 4 shows Arrhenian relations of the diffusion coefficients of Cr parallel to *c*-, *b*-, and *a*-axial directions of orthopyroxene at $f(O_2)$ corresponding to those of the WI buffer.

Table 2
Summary of experimental conditions and Cr diffusion coefficients in enstatite

Diffusion direction	Sample ID	T (°C)	Time (h)	$D(1\sigma)$ ($m^2\ s^{-1}$)	$\log D(1\sigma)$ ($m^2\ s^{-1}$)
$f(O_2)$ = WI ($f(O_2)$ condition corresponding to that of wüstite–iron buffer)					
//*a*	CrEn11a	1000	48	$2.91(0.38)\times10^{-21}$	−20.54(0.06)
	CrEn14a	1100	24	$1.04(0.30)\times10^{-20}$	−19.98(0.12)
				$9.28(2.54)\times10^{-21}$	−20.03(0.12)
//*b*	CrEn08b	900	168	$5.25(2.63)\times10^{-22}$	−21.28(0.22)
				$7.92(3.84)\times10^{-22}$	−21.10(0.21)
	CrEn10b	950	72	$1.50(0.51)\times10^{-21}$	−20.82(0.15)
				$1.79(0.46)\times10^{-21}$	−20.75(0.11)
	CrEn11b	1000	48	$6.68(1.52)\times10^{-21}$	−20.18(0.10)
				$6.29(1.24)\times10^{-21}$	−20.20(0.09)
	CrEn07b	1050	20	$7.18(2.07)\times10^{-21}$	−20.14(0.13)
				$7.28(1.82)\times10^{-21}$	−20.14(0.11)
	CrEn14b	1100	24	$3.09(0.82)\times10^{-20}$	−19.51(0.11)
				$2.42(0.66)\times10^{-20}$	−19.62(0.12)
	CrEn09b	1100	5	$1.97(0.76)\times10^{-20}$	−19.71(0.17)
				$2.81(0.66)\times10^{-20}$	−19.55(0.10)
//*c*	CrEn08c	900	168	$7.17(1.81)\times10^{-22}$	−21.14(0.11)
				$8.45(2.56)\times10^{-22}$	−21.07(0.13)
	CrEn01	950	46	$5.02(0.65)\times10^{-21}$	−20.30(0.06)
				$2.30(0.63)\times10^{-21}$	−20.64(0.12)
				$4.46(0.74)\times10^{-21}$	−20.35(0.07)
	CrEn11c	1000	48	$7.43(0.72)\times10^{-21}$	−20.13(0.04)
				$7.42(0.60)\times10^{-21}$	−20.13(0.03)
	CrEn17	1050	24	$2.06(0.96)\times10^{-20}$	−19.69(0.20)
				$1.99(0.93)\times10^{-20}$	−19.70(0.20)
	CrEn09c	1100	5	$6.20(0.54)\times10^{-20}$	−19.21(0.04)
				$6.39(0.64)\times10^{-20}$	−19.19(0.04)
$f(O_2)$ = WM ($f(O_2)$ condition corresponding to that of wüstite–magnetite buffer)					
//*c*	CrEn02	950	46	$7.41(0.75)\times10^{-21}$	−20.13(0.04)
				$6.44(0.53)\times10^{-21}$	−20.19(0.04)
	CrEn03	950	97	$3.00(0.39)\times10^{-21}$	−20.52(0.06)
	CrEn04	950	192	$2.07(0.21)\times10^{-21}$	−20.68(0.04)
				$2.44(0.19)\times10^{-21}$	−20.61(0.03)
$f(O_2)$ = WI + 3 ($f(O_2)$ condition three orders of magnitude higher than WI buffer)					
//*c*	CrEn13	950	96	$2.94(0.20)\times10^{-21}$	−20.53(0.03)
				$2.98(0.20)\times10^{-21}$	−20.53(0.03)
$f(O_2)$ = WI + 4.5 ($f(O_2)$ condition four and half orders of magnitude higher than WI buffer)					
//*a*	CrEn16a	927	168	$7.79(2.28)\times10^{-22}$	−21.11(0.13)
				$8.52(1.59)\times10^{-22}$	−21.07(0.08)
//*b*	CrEn16b	927	168	$1.14(0.19)\times10^{-21}$	−20.94(0.07)
				$1.22(0.16)\times10^{-21}$	−20.92(0.06)
//*c*	CrEn16c	927	168	$1.40(0.14)\times10^{-21}$	−20.86(0.04)
				$1.86(0.19)\times10^{-21}$	−20.73(0.05)
	CrEn15	1050	49.5	$6.19(1.68)\times10^{-21}$	−20.21(0.12)
				$6.69(1.46)\times10^{-21}$	−20.17(0.09)

The Arrhenian relation is expressed as $D = D_0 \exp(-E/RT)$, where D_0 is a constant and E is the activation energy of diffusion. The vertical bars in Fig. 4 represent $\pm1\sigma$ values of the least squares fits at the selected temperatures. These error bars were calculated according to Tirone et al. (2005) taking into account the covariance of the errors in the slope and intercept values. Least squares fit to the experimental data for diffusion parallel to the *a*-axis is not meaningful as we have experimental data at only two temperatures, 1100 and 1000 °C. Least squares fits to the data for diffusion parallel to *c*- and *b*-axial directions, which are illustrated in Fig. 4 by dashed lines, yield activation energies, $E(\pm1\sigma)$, of 277(±14) and 237(±19) kJ/mol, respectively. However, since $D(//b) < D(//c)$, $E(//b)$ should be greater than $E(//c)$, if one accepts the so-called compensation behavior that suggests a positive linear correlation between $\log D_0$ and E. The validity of the compensation law is, however, a debatable issue, and an insightful discussion of the topic can be found in Lasaga (1998). At any rate, the fact that the least squares fits to the data for diffusion parallel to *c*- and *b*-axial directions yield a lower value of $E(//b)$ than $E(//c)$, instead of the reverse, suggest that the compensation effect, if any, is relatively small compared to the experimental errors of the diffusion data. Thus, we assume

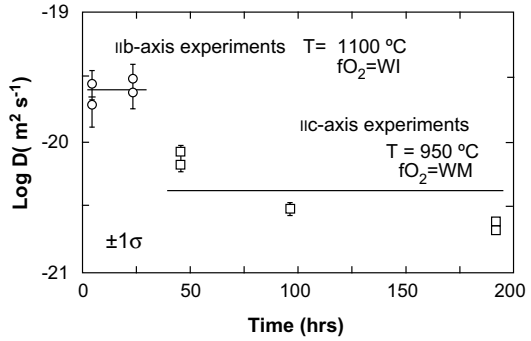

Fig. 2. Time series experiments of Cr diffusion in enstatite parallel to the *b*- and *c*-axial directions at 1 bar and $f(O_2)$ corresponding to that of wüstite–iron (WI) buffer at 1100 °C and wüstite–magnetite (WM) buffer at 950 °C.

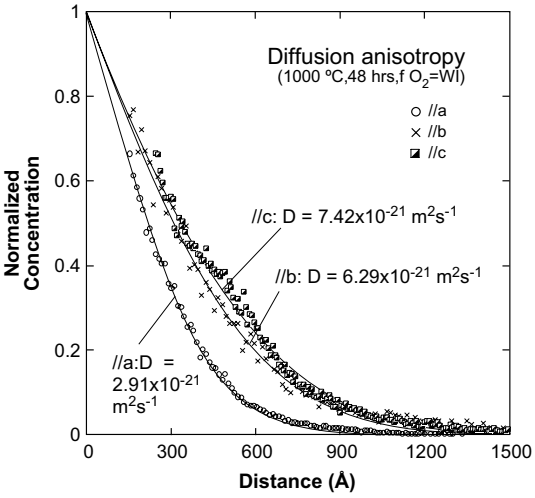

Fig. 3. Anisotropy of Cr diffusion in enstatite, as determined at 1 bar, 1000 °C, $f(O_2) = WI$ buffer condition, by simultaneous annealing of three oriented samples. The symbols indicate the measured count rates, normalized to the surface counts, while the solid lines are fits according to the homogeneous infinite source model.

that the Cr diffusion parallel to different crystallographic directions in orthopyroxene has approximately the same activation energies. Accordingly, we refit the data by constraining the Arrhenian relation to $E = 257(\pm 12)$ kJ/mol that represents the average of $E(//c)$ and $E(//b)$ obtained from the least squares fits to the data sets for diffusion parallel to the *c*- and *b*-axial directions. The results are illustrated as solid lines in Fig. 4. The corresponding $\log D_0$ and D_0 values ($\pm 1\sigma$) are

$$\log D_o(//c) = -9.51(\pm 0.56)\ \mathrm{m^2\ s^{-1}}$$
$$D_o(//c) = 3.10(\pm 3.99)10^{-10}\ \mathrm{m^2\ s^{-1}}$$
$$\log D_o(//b) = -9.75(\pm 0.78)\ \mathrm{m^2\ s^{-1}}$$
$$D_o(//b) = 1.78(\pm 3.19)10^{-10}\ \mathrm{m^2\ s^{-1}}$$
$$\log D_o(//a) = -10.13(\pm 0.39)\ \mathrm{m^2\ s^{-1}}$$
$$D_o(//a) = 7.41(\pm 6.66)10^{-11}\ \mathrm{m^2\ s^{-1}}$$

The standard deviations of $\log D_0$ and D_0 are related according to $\sigma_{D_o} = (2.303 D_o)\sigma_{(\log D_o)}$ (Liermann and Ganguly, 2002).

The diffusion data of Cr parallel to the three crystallographic axes of orthopyroxene, as described by the above relations, are illustrated in Fig. 4d. Compared to the Cr diffusion data in olivine (Ito and Ganguly, 2006) that are illustrated by dashed lines in the figure, D(Cr) in orthopyroxene parallel to either the *c*- or *a*-axial directions is significantly slower, by somewhat more than an order of magnitude at temperatures of interest in planetary problems. There are no data for Cr diffusion in olivine parallel to the *b*-axis. However, from the comparative data for diffusion parallel to the *c*- and *a*-axis, we expect similar difference between the Cr diffusion parallel to the *b*-axis in olivine and orthopyroxene.

3.3. Effect of oxygen fugacity

Ito and Ganguly (2006) did not find any significant change of D(Cr) in olivine for of an increase of $f(O_2)$ condition from that defined by the WI buffer to two orders of magnitude above the buffer ($\log f(O_2) = WI + 2$). It is likely that the range of $f(O_2)$ variation was too small to reveal the effect of $f(O_2)$ on D(Cr) in olivine. In the experiments of Ito and Ganguly (2006), the maximum $\log f(O_2)$ condition was limited to WI + 2 by the maximum attainable flow rate of CO_2 relative to that of CO at which good gas mixing was obtainable. In this work, we were able to attain $\log f(O_2)$ up to WI + 4.5, using a redesigned gas flow system, as discussed above. The effect of variation of $\log f(O_2)$ on D(Cr) parallel to the *c*-axis in orthopyroxene was investigated within the range WI and WI + 4.5. The results, which are illustrated in Fig. 5, show a decrease of $D(Cr//c)$ by a factor of two to three for the increase of $\log f(O_2)$ from WI to WI + 4.5.

The observed effect of $f(O_2)$ on D(Cr) in orthopyroxene is incompatible with a diffusion mechanism mediated primarily by intrinsic vacancies since the concentration of the latter increases with $f(O_2)$, resulting in an increase of the diffusion coefficient. A possible explanation of the observed negative effect of $f(O_2)$ on D(Cr) may lie in the presence of a significant component of interstitial mechanism for the diffusive transport of Cr. The negative correlation between D and $f(O_2)$ was first explained by Dieckmann and Schmalzried (1975) in terms of interstitial mechanism in their study on the effect of $f(O_2)$ on diffusion of Fe in magnetite.

A powder of Cr_2O_3 annealed at 1000 °C for 50 h at the $f(O_2)$ condition of WI buffer did not show any new phase in the X-ray diffraction pattern. Thus, we assume that chromium diffused onto orthopyroxene as Cr^{3+} ion. Following the analysis of Dieckmann and Schmalzried (1975), we can write for interstitial diffusion of Cr^{3+}

$$Cr_o^{3+} + V_i = Cr_i^{3+} + V_o \qquad (a)$$

where Cr_o^{3+} and Cr_i^{3+} denote Cr^{3+} in the octahedral (o) and interstitial sites (i), respectively, and V stands for the vacancies in the indicated sites. The concentration of octahedral vacancies are controlled by the homogeneous

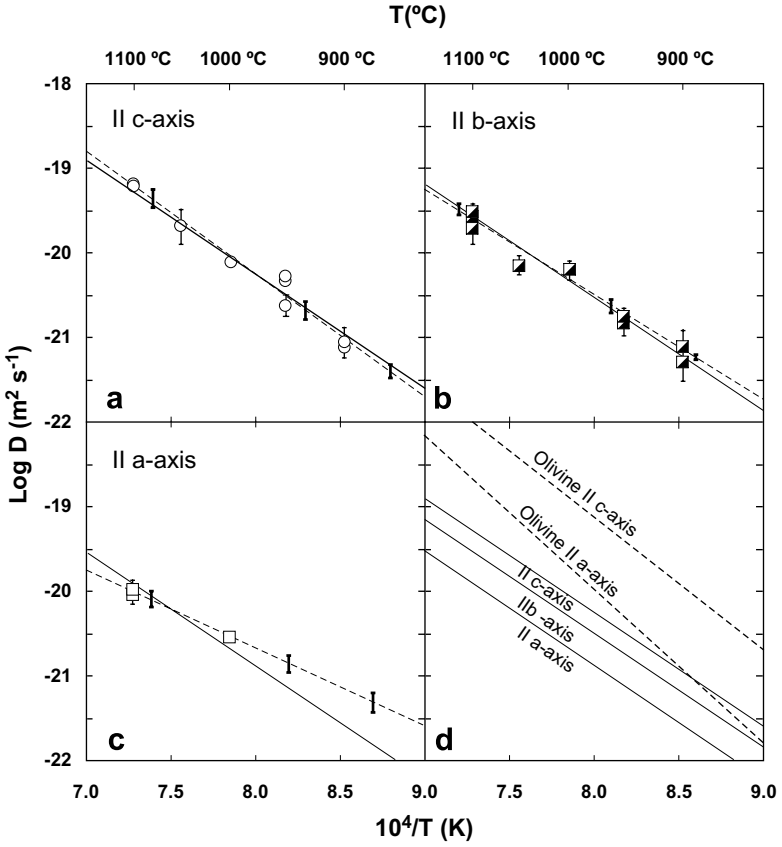

Fig. 4. Arrhenius plots of diffusion coefficient of Cr in enstatite for transport parallel to (a) *c*-axis, (b) *b*-axis, and (c) *a*-axis. Dashed lines represent the least squares or "best fits" to the experimental data, whereas the solid lines represent the "preferred fits" with activation energy constrained by the average of best-fit values for $D(//c)$ and $D(//b)$. The panel (d) shows a comparison of the "preferred fit" Arrhenian relations in enstatite with the Arrhenian relations for $D(//c)$ and $D(//a)$ in olivine, as determined by Ito and Ganguly (2006).

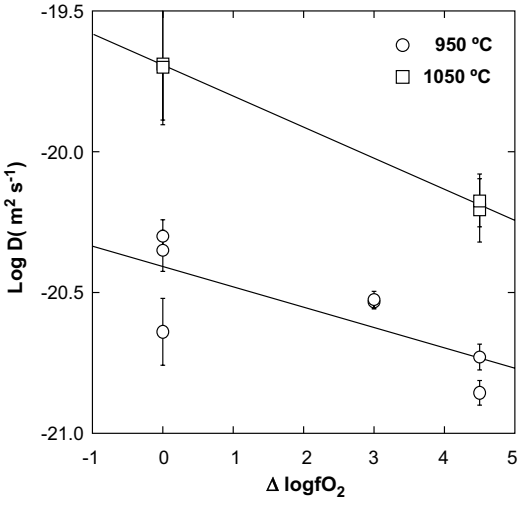

Fig. 5. Dependence of D(Cr) in enstatite on $f(O_2)$, as determined at 950 and 1050 °C. $\Delta\log f(O_2)$ represents the difference between the imposed $\log f(O_2)$ relative to that of wüstite–iron buffer condition.

oxidation reaction of divalent cations, primarily Fe^{2+}, according to

$$3Fe_o^{2+} + 2/3O_2 = 2Fe_o^{3+} + V_o + 1/3Fe_3O_4 \quad (b)$$

Thus, an increase of $f(O_2)$ causes an increase of V_0, which in turn drives the reaction (a) to the left thereby resisting interstitial diffusion. It can be shown from thermodynamic treatment of reactions (a) and (b) that

$$\Delta \log D(\mathrm{Cr}) = -\frac{2}{3}\Delta \log f(O_2) \quad (1)$$

so that for $\Delta\log f(O_2) = 4.5$, $\Delta\log D(\mathrm{Cr}) = -3$, if Cr^{3+} diffuses solely by interstitial mechanism in orthopyroxene. The expected magnitude of decrease of D(Cr) by purely interstitial diffusion mechanism is, however, much larger than what was observed, which is a decrease of D(Cr), not of $\log D$(Cr), by a factor of 2–3. Consequently, there also must be participation of vacancy mediated diffusion to significant extent that counterbalances the effect of interstitial diffusion substantially.

4. CLOSURE-TEMPERATURE AND THERMOCHRONOLOGICAL FORMULATION OF THE ^{53}Mn–^{53}Cr SYSTEM

Ito and Ganguly (2006) have calculated the diffusion closure temperature (T_c) of Cr in olivine as function of initial temperature (T_0), grain size and cooling rate according to the formulation of Ganguly and Tirone (1999). The latter is a modification of the classic Dodson formulation

(Dodson, 1973) removing the assumption of a critical amount of diffusive loss that must be satisfied in order for that formulation to be applicable to natural systems. In the Dodson formulation, T_c depends on cooling rate and grain size. However, as shown by Ganguly and Tirone (1999), if the diffusive loss is insufficient to erase the composition established at T_0 from all parts of a mineral grain, as is often the case for cation diffusion in silicate minerals, then T_c becomes a function of T_0 as well. We have used the Ganguly–Tirone formulation to calculate T_c for Cr diffusion in orthopyroxene as function of T_0, cooling rate at T_c and grain size. These are illustrated in Figs. 6 and 7. As in the Dodson formulation, T vs. t relation is assumed to follow the asymptotic form

$$\frac{1}{T} = \frac{1}{T_o} + \eta t \tag{5}$$

where η is a constant with dimension of $K^{-1}\,t^{-1}$. Thus, the cooling rate at any arbitrary temperature T' is related to that at T_c according to $(dT/dt)_{@T'} = (dT/dt)_{@T_c}(T'/T_c)^2$.

Fig. 6 shows T_c vs. cooling rate at T_c for orthopyroxene grains of spherical geometry with radius varying between 0.5 and 5 mm, and T_0 of 900 and 1100 °C. For these calculations we used average values of the anisotropic diffusion coefficients of Cr parallel to c-, b-, and a-axial directions. The vertical bars show the variation of T_c for change of D from $D(//c)$ to $D(//a)$, with the latter defining the lower limit. Ito and Ganguly (2006) have illustrated T_c vs. cooling rate for diffusion parallel to c- and a-axial directions in olivine grains of spherical geometry. In addition, they have also presented T_c vs. $\log\sqrt{M}$ for spherical geometries at T_0 values of 800, 900, 1000, and 1100 °C, where $\sqrt{M}$ is a dimensionless parameter that can be viewed as an effective diffusion distance normalized to the grain size. The parameter M is defined as

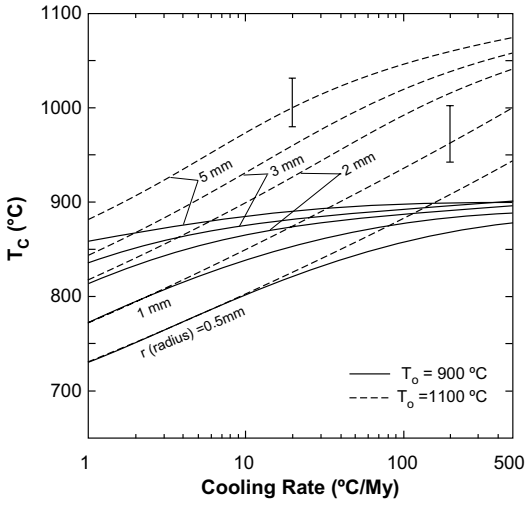

Fig. 6. Closure temperature (T_c) of Cr diffusion in enstatite as a function of initial temperature (T_0), cooling rate and grain size, assuming spherical geometry, and using the average of $D(//c)$, $D(//b)$ and $D(//a)$ values. The vertical bars show the variation of T_c for change of D from $D(//c)$ to $D(//a)$, with the latter defining the lower limit.

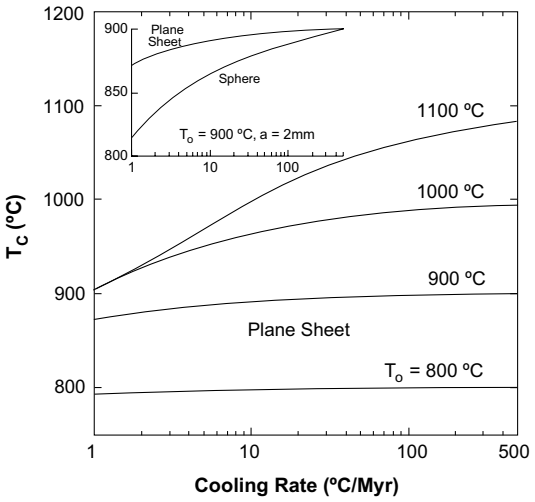

Fig. 7. Main body: Closure temperature (T_c) for Cr diffusion in orthopyroxene vs. cooling rate for the specified initial temperatures (T_0), assuming plane-sheet geometry of enstatite grains with half-width of 2 mm. The inset shows a comparison of the T_c vs. cooling rate relations for plane-sheet and spherical geometries for characteristic grain size (a: radius for sphere and half-width for plane sheet) of 2 mm.

$$M = \frac{RD(T_o)}{E\eta a^2} \tag{6}$$

where $D(T_0)$ is the diffusion coefficient at the peak temperature. The closure temperature, T_c, may be retrieved from these plots for any combination of grain size, cooling rate and diffusion coefficient (since M is dimensionless, these plots are not specific to any mineral).

Fig. 7 shows T_c vs. cooling rate at T_c for specified T_0 values, assuming plane sheet geometry of orthopyroxene grains with half-width of 1 mm. For these calculations we have used the average of $D(//b)$ and $D(//a)$ since orthopyroxene laths are typically parallel to c-axis so that the diffusive loss should take place primarily by transport normal to this axis. The inset of Fig. 7 shows a comparison of T_c for spherical and plane geometries using $T_0 = 900$ °C and a (radius or half-width) = 1 mm. For slowly cooled rocks, the T_c for plane sheet geometry is greater than that for spherical geometry for the same values of T_0, cooling rate and grain size.

Fig. 8 shows a comparison of T_c vs. cooling rate at T_c of the Mn–Cr system in spherical grains of olivine and orthopyroxene for $T_0 = 900$ °C and grain radii of 0.5, 2 and 5 mm that essentially cover the range of variation of grain size of olivine and orthopyroxene in planetary samples. Olivine has a lower T_c than orthopyroxene, but the difference decreases with increasing cooling rate and becomes insignificant for $a \geqslant 2$ mm and cooling rate $\geqslant 50$ °C/Myr. Thus, for relatively rapidly cooled rocks and grain radius of at least 2 mm, olivine and orthopyroxene should define an internal isochron of the Mn–Cr decay system.

During cooling, a mineral grain develops a concentration profile of a decay system (and other species as well), the nature of which depends on the cooling rate, crystal geometry, matrix phases, and the diffusion coefficients of

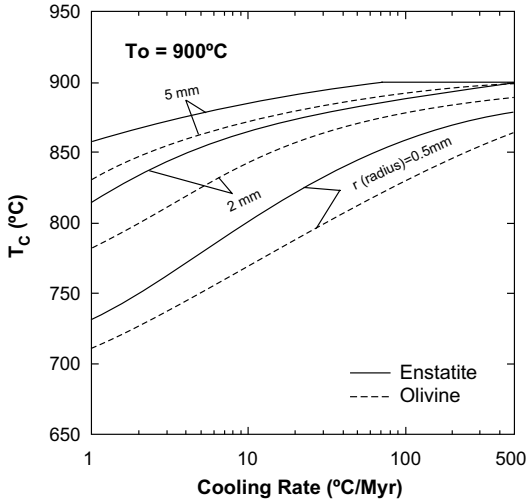

Fig. 8. Comparison of T_c for Cr diffusion vs. cooling rate relations in enstatite and olivine as function of radius of spherical grains of different sizes. The T_c values are calculated using average of D parallel to c-, b-, and a-axis in enstatite and of D parallel to c- and a-axis in olivine. The data for olivine are from Ito and Ganguly (2006) (which also shows more T_c vs. cooling rate and grain size relations for Cr diffusion in olivine).

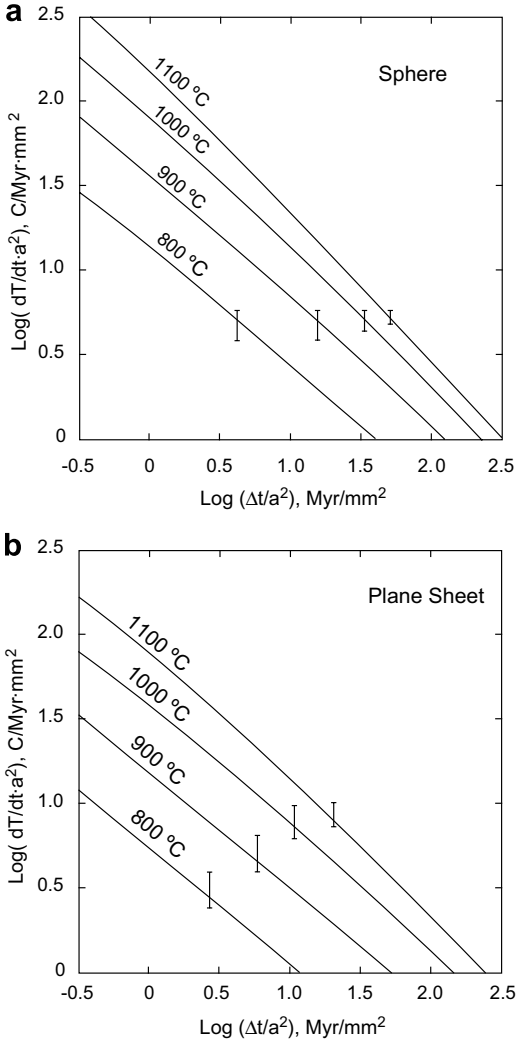

Fig. 9. Cooling rate vs. age loss or resetting (Δt) of the ^{53}Mn–^{53}Cr decay system of enstatite with (a) spherical and (b) plane-sheet geometries. The symbol a in both X- and Y-axis parameters stand for grain size (radius for sphere and half-width for plane sheet). The numbers on the curves indicate the peak temperatures, T_0. The average of D parallel to c-, b-, and a-axial directions is used for the calculation for spherical geometry whereas the average of D parallel to b- and a-axial directions is used for that for plane sheet geometry. The vertical bars indicate the variation of the Y-axis parameter corresponding to the change of diffusion coefficient within the stated limits for the two geometries.

the elements in the mineral of interest and in the matrix. The mineral age that is typically determined by thermal ionization mass spectrometry using crushed grains represents an average of a range of grain size. Ganguly et al. (1998) and Ganguly and Tirone (1999, 2001) showed that cooling rate of a sample can be determined from a knowledge of the average age, average grain size, and the grain geometry (sphere, cylinder, plane sheet). Ito and Ganguly (2006) applied this method to calculate the relationship between cooling rate and resetting of Mn–Cr age of olivine of spherical geometry and specific grain size. Following Ganguly et al. (1998), they presented the results graphically as plots of $\log(\dot{T}a^2) vs. \log(\Delta t/a^2)$ for different values of T_0, where $\dot{T}$ is the cooling rate at T_0, Δt is the extent of resetting of Mn–Cr mineral age, or Mn–Cr age loss during cooling, and a is the grain radius (in general, a is a characteristic dimension of a mineral grain, namely radius of a sphere and cylinder and half-width of a plane sheet).

We have carried out similar calculations for orthopyroxene using both spherical and plane sheet geometries. The results are illustrated in Fig. 9. The curves for spherical geometries are calculated using average Cr diffusivities in orthopyroxenes, but for reasons discussed above, the curves for plane sheet geometry are based on the average of $D(//b)$ and $D(//a)$. A vertical bar on a curve indicates the variation of the Y-axis value resulting from that of D(Cr) between its limiting values.

5. PLANETARY APPLICATIONS

The closure temperatures and the related thermochronological formulations of the Mn–Cr decay system in olivine and orthopyroxene, as presented above and by Ito and Ganguly (2006), provide the major foundation for the quantitative interpretation of Mn–Cr mineral ages in early solar system objects. However, with a few exceptions, all Mn–Cr age data for planetary samples represent whole rock data. Our study shows that important thermochronological information may be extracted for the early planetary accretion and differentiation processes if Mn–Cr mineral age data for controlled grain sizes become available. Using the data from Lugmair and Shukolyukov (1998) for the Mn–Cr age of olivine in a pallasite, Omolon, which is a stony-iron meteorite, Ito and Ganguly (2006) calculated its cooling rate and thereby the burial depth, which represents the core-mantle boundary of the parent body. It

was concluded that the pallasite Omolon was buried at ~30 km depth in a parent body of at least ~100 km radius. In this work, we use the Mn–Cr age of orthopyroxenes from a cumulate Eucrite, Serra de Magé, to constrain their cooling rates in situ, and thereby the minimum thickness of the eucrite crust in the parent body.

5.1. Cooling rate of Serra de Magé: minimum thickness of eucrite crust in HED parent body

Lugmair and Shukolyukov (1998) determined the ^{53}Cr excess in chromite and pyroxene grains from a cumulate eucrite, Serra de Magé, and thereby determined an Mn–Cr mineral age of 4553 (+2/−4) Ma. As noted by them, this age is considerably older than the ^{147}Sm–^{143}Nd age of 4410 ± 20 Ma for this meteorite (Lugmair et al., 1977), which implies that the Mn–Cr system closed relatively early in the parent body history, while the Sm–Nd age dates a secondary event.

The eucrites belong to a group of achondrites, the howardite–eucrite–diogenite or HED suite, which is usually considered to have been derived from the asteroid 4 Vesta (McCord et al., 1970; Consolmagno and Drake, 1977; Gaffey, 1993). Eucrites constitute the basaltic upper crustal rocks in the HED parent body, and are subdivided into two groups, cumulate eucrites and basaltic eucrites. The basaltic crust is overlain by howardites that are polymict breccia containing fragments of eucrites and diogonites. The latter constitute the lower crust and represent the refractory residue (primarily orthopyroxene with minor quantities of olivine and chromite) of the parent material after extraction of the partially molten basaltic component to form the upper crust.

From analysis of the Mn/Cr ratio and ^{53}Mn–^{53}Cr chronological data of the HED parent body, Lugmair and Shukolyukov (1998) inferred a time lapse of ~3.2 Myr between the time of origin of the solar system (4568 Ma, according to these authors) and the time of HED mantle differentiation. Thus, we conclude that the orthopyroxene crystals in the cumulate eucrites crystallized ~4564.8 Ma. The difference between this crystallization age and the Mn–Cr closure age of orthopyroxene (4553 (+2/−4) Ma), which is ~10–16 Myr, then corresponds to the age loss or resetting of the Mn–Cr decay system in orthopyroxene during cooling within the HED parent body. Here we are interested in determining the cooling rate of the cumulate eucrite sample in situ in the HED parent body from the age loss of the Mn–Cr decay system in orthopyroxene, and thereby to constrain its burial depth. However, prior to ejection out of the parent body, chunks of the meteorite samples were excavated from depth, and buried under a regolith blanket (Liermann and Ganguly, 2001). Thus, we need to evaluate if part of the Mn–Cr age loss of Serra de Magé is a result of cooling under a regolith blanket.

Following the theory of Mueller (1967) and the numerical method of Ganguly (1982), Domeneghetti et al. (1996) determined the cooling rates of eucrite samples, including Serra de Magé, on the basis of the Fe^{2+}–Mg ordering between the non-equivalent octahedral sites, M2 and M1, in orthopyroxene. They inferred a cooling rate of the order of 10^3 °C/Myr for the eucrite samples. These data reflect near surface cooling under a regolith blanket. Using orthopyroxene grain radii of 0.5 to 5.0 mm, we obtain M (defined by Eq. 6) $= 5.2(10^{-4}) - 5.2(10^{-6})$ for $T_0 = 900$ °C, and $M = 2.6(10^{-3}) - 2.6(10^{-5})$ for $T_0 = 1000$ °C. Comparison of these data with the T_c vs. $\log\sqrt{M}$ for fixed values of T_0 calculated by Ito and Ganguly (2006) for spherical geometries, for which the diffusive loss is maximum, shows that no resetting of the Mn–Cr age of orthopyroxene was possible during rapid cooling at a rate of ~1000 °C/Myr under a regolith blanket in the HED parent body. Thus, the entire resetting of ~10–16 Myr of the Mn–Cr system in Serra de Magé studied by Lugmair and Shukolyukov (1998) must have been due to cooling at the original site of the sample in the parent body.

On the basis of experimental phase equilibrium data, Stolper (1977) concluded that the pyroxenes in Serra de Magé crystallized at a temperature less than 1140 °C when the sample was 45–65% crystalline. Thus, for the purpose of cooling rate calculations from the Mn–Cr age resetting of orthopyroxenes, we assume $T_0 = 1000$–1100 °C. Lugmair and Shukolyukov (1998) did not report the grain size of orthopyroxene crystals that they analyzed, nor they are in a position to determine it now (Lugmair and Shukolyukov, personal communication). However, from observations of the orthopyroxene grains in the eucrite samples, we conclude that the grain size of orthopyroxene crystals falls in the range of 0.5–5.0 mm radius. This range of grain size and the inferred age loss (Δt) of ~10–16 Myr for the Mn–Cr decay system in the orthopyroxenes in the Serra de Magé yield, according to the cooling rate vs. age relations illustrated in Fig. 9a, an average cooling rate of ~4–27 °C/Myr at T_c at the original site of the sample in the HED parent body, if the grains are assumed to be approximately spherical. Plane sheet geometry (Fig. 9b) yields a cooling rate of ~2–20 °C/Myr. Thus, we conclude that Serra De Magé cooled at a rate of ~2–27 °C/Myr at its original site within the upper crust in the parent body.

Using T_0 of 1000–1100 °C, cooling rate of 2–27 °C/Myr, and age loss of 10–16 Myr, we obtain $T_c = 830$–980 °C for the Serra de Magé orthopyroxenes. From Fe^{2+}–Mg fractionation data between orthopyroxene and spinel in Serra de Magé, Liermann and Ganguly (2001) calculated a temperature of 715 °C for the closure of Fe–Mg exchange between orthopyroxene and spinel. Since $D(Cr) < D(Fe–Mg)$ in orthopyroxene (according to this study and Schwandt et al., 1998), the T_c for Cr diffusion should be higher than that of Fe–Mg inter-diffusion for similar set of conditions. Thus, the retrieved T_c values for Cr and Fe–Mg diffusion in orthopyroxene are compatible with those expected from the diffusion kinetic properties of the two systems.

Since cooling to the closure temperature of Cr in orthopyroxene must have taken place in the rocky crustal material, as discussed above, we can use the inferred cooling rate to constrain the depth of burial of Serra de Magé. For this purpose, we use the graphical relationship presented by Wood (1979) between the radius of a

spherical parent body (R) and the depth of burial of an excavated sample as function of T_0 and cooling rate at 500 °C. The asymptotic cooling model used in this work, Eq. 5, yields a cooling rate of ~1–13 °C/Myr at 500 °C, corresponding to the calculated cooling rate of 2–27 °C/Myr at T_c (830–980 °C). If we accept asteroid Vesta as the parent body of eucrites, then $R = 400$ km. This combination of cooling rate at 500 °C and R yields a burial depth of ~30 km for the cumulate eucrite Serra de Magé. Thus, we conclude that the thickness of the eucrite upper crust is greater than 30 km.

There are several models of the internal lithological structure of Vesta that have been reviewed by Ruzicka et al. (1997). Some of the models (Mason, 1967; Delaney, 1995) propose a thickness of the eucrite crust that is less than what has been inferred above. Ruzicka et al. (1997) propose several models depending on the core mass (0–25% of the total), and the amount of olivine constituting the mantle of the asteroid. The minimum thickness of the eucrite crust derived above is compatible with a relatively olivine-poor model in which olivine constitutes 19.7% of the total asteroidal mass, with the core mass varying between 0% and 25% of the total.

ACKNOWLEDGMENTS

The research was supported by a NASA Cosmochemistry grant NNG04GG26G, and a post-doctoral fellowship to M.I. from the Japan Society for Promotion of Sciences (JSPS). We deeply appreciate the generosity of Prof. N. Sugiura and Dr. A. Miyazaki for making their SIMS facility at the University of Tokyo available for this project while M.I. has been at the same University on the JSPS fellowship. Thanks are due to Prof. Richard Hervig for allowing us access to the SIMS facility of the Arizona State University and advice on analytical procedures. The careful reviews by Dr. Daniele Cherniak, Prof. Andy Davis and an anonymous reviewer, and the editorial handling of Dr. Rick Ryerson are gratefully acknowledged.

REFERENCES

Consolmagno G. J. and Drake M. J. (1977) Composition and evolution of the eucrite parent body—evidence from rare earth elements. *Geochim. Cosmochim. Acta* **41**, 1271–1282.

Crank J. (1975) *The Mathematics of Diffusion*, 2nd ed. Oxford University Press, Oxford.

Delaney J. S. (1995) 4 Vesta: a thick-skinned parent for basaltic achondrites. *Lunar Planet. Sci. XXVI* Lunar Planet. Inst., Houston, pp. 329–330.

Dieckmann R. and Schmalzried H. (1975) Point defects in oxide solid solutions: (III) Mobilities of cations and vacancies in (Co,Ni)O- and (Co,Mg)O-solid solutions and the calculation of correlation factors. *Ber. Bunsenges. Phys. Chem.* **79**, 1108–1115.

Dodson M. H. (1973) Closure temperature in cooling geochronological and petrological systems. *Contrib. Mineral. Petrol.* **40**, 259–274.

Domeneghetti M. C., Tazzoli V., Ballaran T. B. and Molin G. M. (1996) Orthopyroxene from the Serra de Magé meteorite: a structure-refinement procedure for a Pbca phase coexisting with a C2/c exsolved phase. *Am. Mineral.* **81**, 842–846.

Gaffey M. J. (1993) Forging an asteroid-meteorite link. *Science* **260**, 167–168.

Ganguly J. (1982) Mg–Fe order-disorder in ferromagnesian silicates: II. Thermodynamics, kinetics and geological applications. In Advances in Physical Geochemistry (ed. S. K. Saxena). Springer-Verlag, New York, USA, pp. 88–99.

Ganguly J. and Tazzoli V. (1994) Fe^{2+}–Mg interdiffusion in orthopyroxene: Retrieval from the data on intracrystalline exchange reaction. *Am. Mineral.* **79**, 930–937.

Ganguly J. and Tirone M. (1999) Diffusion closure temperature and age of a mineral with arbitrary extent of diffusion: theoretical formulation and applications. *Earth Planet. Sci. Lett.* **170**, 131–140.

Ganguly J. and Tirone M. (2001) Relationship between cooling rate and cooling age of a mineral: theory and applications to meteorites. *Meteor. Planet. Sci.* **36**, 167–175.

Ganguly J., Tirone M. and Hervig R. L. (1998) Diffusion kinetics of Samarium and Neodymium in garnet, and a method for determining cooling rates of rocks. *Science* **281**, 805–807.

Hutcheon I., Krot A. N., Keil K., Phinney D. L. and Scott E. R. D. (1998) ^{53}Mn–^{53}Cr dating of fayalite formation in the CV3 chondrite Mokoia: Evidence for asteroidal alteration. *Science* **282**, 1865–1867.

Ito M. and Ganguly J. (2004) Potassium diffusion in melilite: Experimental studies and constraints on the thermal history and size of planetsimals hosting CAIs. *Meter. Planet. Sci.* **39**, 1911–1919.

Ito M. and Ganguly J. (2006) Diffusion kinetics of Cr in olivine and ^{53}Mn–^{53}Cr thermochronology of early solar system objects. *Geochim. Cosmochim. Acta* **70**, 799–806.

Lasaga A. C. (1998) *Kinetic Theory in the Earth Sciences*. Princeton, New Jersey.

Liermann H-P. and Ganguly J. (2001) Compositional properties of coexisting orthopyroxene and spinel in some Antarctic diogenites: Implications for thermal history. *Meteor. Planet. Sci.* **36**, 155–166.

Liermann H-P. and Ganguly J. (2002) Diffusion kinetics of Fe^{2+} and Mg in aluminous spinel: experimental determination and applications. *Geochim. Cosmochim. Acta* **66**, 2903–2913.

Lugmair G. W., Scheinin N. B. and Cralson R. W. (1977) Sm–Nd systematics of the Serra de Magé eucrite. *Meteoritics* **12**, 300–301.

Lugmair G. W. and Shukolyukov A. (1998) Early solar system timescales according to ^{53}Mn–^{53}Cr systematics. *Geochim. Cosmochim. Acta* **62**, 2863–2886.

Mason B. (1967). *Meteorites American Scientist* **53**, 429–455.

McCord T. B., Adams J. B. and Johnson T. V. (1970) Asteroid Vesta: spectral reflectivity and compositional implications. *Science* **168**, 1445–1447.

McKeegan K.D. and Davis A.M. (2004) Early solar system chronology. In Meteorites, Comets, and Planets. Treatise on Geochemistry, vol. 1 (ed. A. M. Davis). Elsevier-Pergamon, Oxford, pp. 431–460.

Mueller R. F. (1967) Model for order-disorder kinetics of certain quasi-binary crystals of continuously variable composition. *J. Phys. Chem. Solids* **18**, 2239–2243.

Nyquist L., Lindstrom D., Mittlefehldt D., Shih S-H., Wiesmann H., Wentworth S. and Martinez R. (2001) Manganese–chromium formation intervals for chondrules from the Bishunpur and Chainpur meteorites. *Meteor. Planet. Sci.* **36**, 911–938.

Ruzicka A., Snyder G. A. and Taylor L. A. (1997) Vesta as the howardite, eucrite and diogenite parent body: implications for the size of a core and for large-scale differentiation. *Meteor. Planet. Sci.* **32**, 825–840.

Schwandt C. S., Cygan R. T. and Westrich H. R. (1998) Magnesium self-diffusion in orthoenstatite. *Contrib. Mineral. Petrol.* **130**, 390–396.

Stolper E. (1977) Experimental petrology of eucrite meteorites. *Cosmochim. Acta* **41**, 587–611.

Sugiura N. (2002) Mn–Cr chronology of olivine in some meteorites. *Lunar Planet. Sci. XXXIII*, Lunar Planet. Inst., Houston, CD-ROM#1435.

Tirone M., Ganguly J., Dohmen R., Langehorst F., Hervig R. L. and Becker H-W. (2005) Rare earth diffusion kinetics in garnet: experimental studies and applications. *Geochim. Cosmochim. Acta* **69**, 2385–2398.

Wood J.A. (1979) Review of the metallographic cooling rates of meteorites and a new model for the planetesimals in which they formed. In Asteroids, University of Arizona Press, Tucson, Arizona, pp. 849–891.

Associate editor: F.J. Ryerson